Active Reflection Coefficients Optimization for Antenna Arrays

Chrysovalantis Stefopoulos, Mario Coutino, *Member, IEEE*, Peter de Hek, *Member, IEEE*, Dave Bekers, *Senior Member, IEEE*, Ioannis Iliopoulos, Stefania Monni, *Senior Member, IEEE*

***Abstract*—This paper addresses the challenge of enhancing the power radiated by Active Electronically Scanned Array (AESA) radars, in particular at large scan angles, where performance degradation arises from both the cosine-dependent reduction in antenna effective area and suboptimal active impedance matching. Traditional methods to improve directivity—such as increasing the number of elements, employing asymmetric element designs, or integrating bulky lens systems—present various trade-offs that can compromise overall system efficiency. Here, we explore an approach that increases the radiated power by optimizing the active reflection coefficients (ARCs) of the antenna through the synthesis of array element excitations. Focusing on a planar dipole array, we compare stochastic differential evolution and convex optimization techniques, under the constraint of a uniform amplitude taper, which is critical to limit the loss in output power. Furthermore, we combine this with a quasi-balanced Doherty power amplifier architecture that compensates for the remaining scan-angle-induced variations in output load impedance. The study includes a detailed analysis of the effects of phase and amplitude errors on ARC control and demonstrates, through numerical results, the improved performance of the integrated system over conventional designs.**

***Index Terms*—phased arrays, antenna arrays, reflection coefficient, antenna radiation patterns, high power amplifiers, energy efficiency, integrated design**

I. Introduction

THE sensitivity of an Active Electronically Scanned Array (AESA) radar, calculated by using the radar equation [1], depends on the radiated power and changes with the direction of observation. The latter is mainly due to the geometrical decrease of the antenna effective area (and thus the directivity) according to the cosine of the pointing angle, and to the deterioration of the active impedance matching with scanning [2].

Several approaches can be devised to enhance the directivity of the antenna. The number of antenna elements in the array could be increased, depending on the space available on the platform, but this results in: i) a smaller beamwidth which will ask for either beam spoiling or a different time-energy budget to cover a given angular volume and ii) an increased costs due to the acquisition, control and processing of the extra elements, which may not always be desirable. Radiating elements with an asymmetric active element pattern could be designed to provide a higher directivity for large pointing angles. However, often such elements require undersampling the array aperture ($> \lambda/2$) [3], leading to grating lobes and sensitivity loss. The array could be equipped with a lens to obtain an additional phase shift at the edge of the field of view [4], but such a solution results in relatively bulky architectures.

The focus of this paper is on increasing the radar sensitivity and reducing the power dissipation by improving the AESA active impedance matching. AESA radars are evolving towards fully digital systems, with signal generation at each element, which will enable a great degree of flexibility in the implementation of different functionalities, at element and sub-aperture level [5]–[7]. A tile-type of architecture is foreseen, with digitization of the signal at element level and a complete Transmit/Receive (TR) module per unit cell. The circulator-isolator between the antenna, one of the largest components in the TR module, will be replaced by a switch. Thus, in the transmit chain the High Power Amplifier (HPA) will be directly exposed to the variation of the antenna Active Reflection Coefficients (ARCs) with scan angle [8] with two main effects: on the RF performance, namely the Power Added Efficiency (PAE) and the output power made available at the antenna port, and hence, on the dissipated power, which in turn limits the maximum output power [9].

The problem of controlling the ARCs of a scanning AESA antenna can be addressed at radiating element level, e.g. [10]; through wide angle impedance matching superstrates, e.g. [11]; through adaptive matching circuits at the antenna feed, e.g. [12]; by implementing compensation schemes based on connecting circuits, e.g. [13], [14]. However, these approaches add complexity to the design of the antenna elements or the overall array architecture, since most of them require the inclusion of reconfigurable technology to adjust the phase when scanning.

Optimization methods are commonly used for the radar receiver, e.g., to support the implementation of digital beamforming approaches [21]–[23], with various objectives ranging from equalizing the embedded-elements patterns across the array to beam broadening or spoiling and sidelobe reduction and nulling. However, the literature on the use of such methods to minimize the ARCs of transmit-array elements is limited. Recently, several ARC reduction methods have been proposed which generate appropriate antenna-elements excitations through constrained optimization [15], [16], through precoder designs [17], [18], and through a waveform synthesis technique [19]. In this paper we will focus on the optimization methods. In [15] two types of objective functions for minimizing the ARC are investigated, where one can be handled by a gradient-based algorithm, using Matlab's optimization function 'fminunc', and the other can be handled by a stochastic algorithm, using an own implementation of

Corresponding author: Chrysovalantis Stefopoulos (e-mail: chrysovalantis.stefopoulos@tno.nl). C. Stefopoulos, M. Coutino, D. Bekers and P. de Hek are with TNO, 2597 AK The Hague, The Netherlands. S. Monni is with TNO, 2597 AK The Hague, The Netherlands, and also with the Eindhoven University of Technology, 5612 AZ Eindhoven, The Netherlands (e-mail: stefania.monni@tno.nl).

This paper is an expanded version from the 2024 IEEE International Symposium on Phased Array Systems and Technology, Boston, MA USA, 15-18 October 2024.

differential-evolution (DE). Stochastic optimization algorithms are frequently desired when the objective function is not differentiable or requires numerical differentiation. But, while gradient-based algorithms have convergence guarantees, such guarantees are not readily available for stochastic algorithms. Also, gradient-based algorithms require differentiability of the objective function and, potentially, of the constraints.

For these reasons we build in this paper on our earlier effort [16], where we introduced an alternative formulation of minimizing the ARCs with pattern constraints, which allows using convex optimization techniques. In particular, we derive a semi-definite programming formulation, which can be handled by the Matlab plug-in CVX [20]. Like gradient-based algorithms, the convex optimization techniques are local and require thus a prescribed 'start solution'. However, the objective and constraints need to have a semi-definite programming formulation instead of being differentiable. An advantage of convex optimization is the smoothness of the convergence graphs, which provides a means of predicting the number of iterations needed to achieve a certain level of ARC, as shown in [16].

In this paper, we revisit briefly our work in [16] and add computational details that make our method more memory efficient and a pseudo code for ease of implementation. Also, we add a brief description of the stochastic DE method. Next, we compare the results of the stochastic and convex optimization methods for a planar array of dipoles, where we employ an own implementation of the DE method and a Matlab implementation of our pseudo code, which calls the Matlab package CVX [20]. In [15] both the amplitude and phase of the excitations are designed, giving an additional degree of freedom in the minimization of the ARC. In this paper, targeting radar applications where the HPA works in saturation, a uniform amplitude taper is assumed and, hence, the optimization methods are designed and implemented in such a way that only on the phase of the excitations is tuned. The effect of phase and amplitude errors in the antenna-elements excitations, as well the application of the optimization procedure over multiple frequencies is also discussed. Moreover, while [15] and [16] present only the synthesis of appropriate antenna-elements excitation schemes with minimized ARCs, in this paper a HPA architecture is presented that can compensate for the remaining variations of the output load impedance, i.e., the antenna active impedance, based on a Quasi Balanced Doherty Power Amplifier (QB-DPA). Finally, the performance of such a HPA concept in combination with the array antenna equipped with the synthesized excitations is analyzed and compared with that of the original array.

The paper is structured as follows. In Sec. II a breakdown of the problem is presented, as well as the devised solution approach, including the considered HPA architecture. In Sec. III the investigated optimization techniques for the antenna-array excitations are outlined and their performance analysed mainly for an array of dipoles. Numerical results are reported in Sec. IV , both the stand alone antenna and the antenna combined with the proposed HPA architecture. Main conclusions are reported in Sec. V.

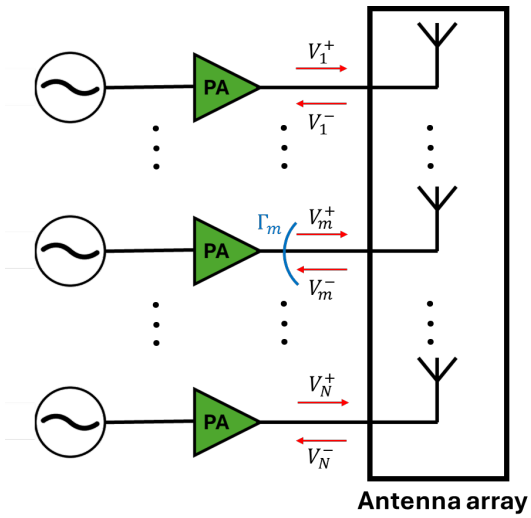

Fig. 1. Mutual coupling effects in a linear array of N elements.

II. Active Reflection Coefficients and High Power Amplifier Design

In the following, we present the formulation of the ARCs for antenna arrays and provide a design strategy for HPAs tailored to compensate for coupling-induced load variations. First, we detail how the ARCs – essential parameters that encapsulate both the self-reflection of individual antenna elements and their mutual coupling – can be optimized while satisfying stringent radiation pattern and gain requirements. Next, we explore a HPA strategy, based on the QB-DPA architecture, that dynamically adapts to the changing load conditions imposed by the array's scanning behavior, thereby preserving output power and efficiency, and preventing thermal overload. Finally, the section outlines the design flow employed in this work for generating the simulation results.

A. Antenna Active Reflection Coefficient Design

Let us first consider a linear array of N antenna elements with V_m^+ denoting the incident voltage at the port of the m-th element and V_m^- the voltage reflected towards the same element, as illustrated in Fig. 1. Then, the scattering parameters of the array, which are a measure of the mutual coupling, are defined by

$$S_{mn} = \left.\frac{V_m^-}{V_n^+}\right|_{V_k^+=0 \; for \; k\neq n} \tag{1}$$

If the incident voltages have amplitudes a_m and phases φ_m to direct the array beam in scan direction (θ_0, ϕ_0), then

$$V_m^+ = a_m e^{j\psi_m} \tag{2}$$

Note that, if the time-harmonic factor is $e^{-j\omega t}$ and if mutual coupling is ignored in a planar array, ψ_m assumes the well-known expression

$$\psi_m = -k\left(x_m \sin\theta_0 \cos\phi_0 + y_m \sin\theta_0 \sin\phi_0\right) \tag{3}$$

where k is the wave number and x_m and y_m are the Cartes coordinates of element m. The total voltage at the n antenna port is expressed as

$$V_m = V_m^+ + V_m^- = V_m^+ \left(1 + \frac{1}{V_m^+} \sum_{n=1}^{N} S_{mn} V_n^+\right) = \\ = a_m e^{j\psi_m} \left(1 + S_{mm} + \frac{1}{a_m} \sum_{n=1, n\neq m}^{N} S_{mn} a_n e^{j(\psi_n - \psi_m)}\right) \tag{4}$$

The ARC at the m-th element for the scan direction (θ_0, ϕ_0), $\Gamma_{\theta_0,\phi_0,m}$, follows straightforwardly as

$$\Gamma_{\theta_0,\phi_0,m} = \frac{V_m^-}{V_m^+} = \\ S_{mm} + \frac{1}{a_m} \sum_{n=1, n\neq m}^{N} S_{mn} a_n e^{j(\psi_n - \psi_m)} \tag{5}$$

The ARC of a certain array element thus depends on the relative excitation amplitudes and phases, and on the coupling coefficients. The ARCs can be expressed in a matrix-vector form as

$$\mathbf{\Gamma}_{\theta_0,\phi_0} = \mathrm{diag}\left(\mathbf{a}(\theta_0,\phi_0)^{\odot -1}\right) \mathbf{S}\, \mathbf{a}(\theta_0,\phi_0) \in \mathbb{C}^N \tag{6}$$

where $\mathbf{S}$ is the $N \times N$-scattering matrix of an antenna array consisting of N elements, $\mathbf{a}(\theta_0, \phi_0)$ is the vector of the complex excitation coefficients of the N antenna elements to scan in the direction (θ_0, ϕ_0), and $\mathbf{\Gamma}_{\theta_0,\phi_0}$ is the corresponding vector of ARCs.

Given the relation between the ARCs of the antenna elements and the reflected power, the design and optimization of the elements' excitations should aim at minimizing the reflected power if higher efficiencies are desired, or, at high-power operation, if effects of load pull and heating are too pronounced. Although excitations values that minimise the ARCs levels are targeted, the antenna array has also to maintain the prescribed radiation characteristics. For this purpose, constraints are imposed on its (i) gain and (ii) radiation pattern – in terms of sidelobe level. The objective of minimizing the ARCs and the constraints on gain and sidelobe level can be formulated

$$\begin{aligned} \min_{\mathbf{a}\in\mathbb{C}^N} \quad & \|\mathbf{\Gamma}_{\theta_0,\phi_0;\mathbf{a}}\|_\infty \\ \text{s.t.} \quad & G(\theta_0,\phi_0;\mathbf{a}) \geq G_{\text{spec}} \\ & \max_{(\theta,\phi)\in\Theta} SLL(\theta,\phi;\mathbf{a}) \leq SLL_{\text{spec}} \\ & \|\mathbf{a}\|_2 = 1 \end{aligned} \tag{7}$$

where the infinity norm, i.e., $\|\cdot\|_\infty$ denotes the maximum absolute component of a vector, $\|\cdot\|_2$ is the Euclidean norm, G and SLL denote gain and sidelobe level, and the subscript $_{\text{spec}}$ denotes specification. The last constraint, which one could interpret as uniform excitation power over the array, has been introduced to fix the invariance of the problem with respect to a complex constant. Note that the SLL and the gain are invariant with respect to the multiplication by a complex constant. Methods to tackle (7) are discussed in Section III.

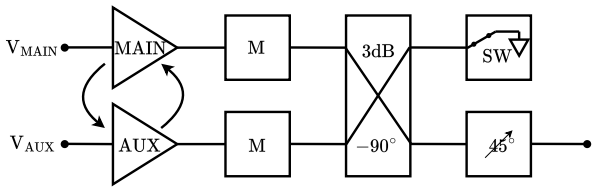

Fig. 2. Block diagram of the QB-DPA considered for this study.

B. High Power Amplifier Design

The use of HPAs in an AESA environment without a circulator or isolator between the HPA and the antenna leads to a variation in amplifier performance parameters, such as output power and efficiency, as a function of the scan direction due to the corresponding variation of the ARCs at the HPAs output caused by the mutual coupling. These variations will also lead to an increase in power dissipation and, consequently, to a temperature increase of the HPAs [9]. Such temperature increases can become so high that the lifetime of the amplifier is severely compromised. Therefore, amplifier concepts were studied that, for a given load impedance, can:

- set the required output power level, so that the antenna elements are excited with the specified input power,
- restore the efficiency as good as possible, so that the reduction in life time is minimized.

From the literature a number of concepts are known that can fulfill the aforementioned requirements. For this work, the Quasi Balanced Doherty Power Amplifier (QB-DPA) concept [28]–[30] was chosen. Its block diagram is depicted in Fig. 2. This concept was selected because of its capability to fully compensate for variations in the real part of its load impedance and partly compensate for variations in its imaginary part. In the Doherty concept, the active load modulation is used to set the output power and correct the efficiency as much as possible to its intended value for a given load impedance. This architecture consists of a main and an auxiliary amplifier, see Fig. 2, with two inputs that can be controlled independently. The input magnitudes are used to control the output currents of the amplifiers and their phase difference is set in such a way that the desired output power, efficiency, and insertion phase are achieved.

In the one-stage design of the main and auxiliary amplifier, see Fig. 2, two identical transistors are used. These transistors are modeled as ideal current sources, controlled via their input voltage. In addition, these currents are made dependent on their output voltages. The current can be shown to be described by

$$I_D(V_G, V_D) = \frac{G_{\text{MAX}}}{2} \Bigg\{ V_G - V_T + \frac{1}{\alpha} \log \Big[\\ 2\cosh\left(a\left(V_G - V_T\right)\right) \Big] \Bigg\} \tanh\left(\frac{2V_D}{V_K}\right) \tag{8}$$

where V_G and V_D are the gate and drain voltages respectively. The following values have been used for the results of this paper:

- threshold voltage $V_T = -3$ V
- knee voltage $V_K = 0.01$ V
- tuning parameter $\alpha = 10$ V^{-1}
- maximum trans-conductance $G_{\mathrm{MAX}} = 250\mathrm{mS/mm}$

Here, we have used a typical value for V_T for a GaN process. Note that the knee voltage has been deactivated to corroborate that in the ideal case the theoretical class B efficiency of $\pi/4$ is maintained.

As illustrated in Fig. 2, there are two identical matching networks M behind the amplifiers. These matching networks transform the $50\ \Omega$ input impedance of the quadrature coupler into the optimum load impedance of the transistors. The coupler is assumed to be lossless, with infinite isolation, and a reference impedance of $50\ \Omega$.

The efficiency of the main amplifier, see Fig. 2, is maximized by always keeping the RF output voltage swing, or range of the output voltage, and the DC supply voltage constant. To avoid clipping, the DC voltage of the auxiliary amplifier is modified so that it can accommodate its RF voltage swing. It has been shown [31] that, if all possible load impedances should be compensated for a series Doherty amplifier, large DC voltages might be needed to avoid clipping. Depending on the breakdown voltage of the considered semiconductor technology this limits the possible output power of the amplifier. As illustrated in [28] and [29], to keep the DC voltages manageable, the amplifier is switched, for a given impedance range, from a series Doherty amplifier to a parallel one by switching the impedance at the isolated port of the quadrature coupler from a short to an open. At the same time, the role of the main and auxiliary amplifier and their DC supply voltages is interchanged.

Across this work, the output power in a $50\ \Omega$ load impedance is required to be 100 W. To achieve this output power, the output peak current of the amplifiers is tuned to 4 A, at a supply voltage of 50 V. Also, the amplifiers are operated in class B and, since the knee voltage of the transistors is set to $V_K = 0.01$ V, the efficiency is approximately 78.5%. In the amplifier design of this paper, the following modifications have been introduced with respect to [29] and [30]:

- Adaptation of the DC supply voltage of the auxiliary amplifier is done in such a way that no clipping of the voltage waveform occurs and as a result its efficiency is maximized
- Addition of a $45°$ phase shifter at the output of the amplifier to be able to select a favorable phase of the load reflection coefficient of the internal transistors depending on the phase of the external load reflection coefficient.

With respect to the second item we need to say that our ARC design problem (7) assumes antenna excitations with equal amplitude voltages and, hence, the output power $P_{m,\mathrm{OUT}}$ of the m-th amplifier needs to vary as a function of its active reflection coefficient $\Gamma_{\theta_0,\phi_0,m}$ as

$$P_{m,\mathrm{OUT}}(\theta_0,\phi_0) = |a_m|^2\left(1-|\Gamma_{\theta_0,\phi_0,m}|^2\right) \tag{9}$$

To illustrate the effect of the added phase shifter, an example of efficiency plots with and without the phase shifter is shown in Fig. 3. Here, one can observe an improvement of the minimum

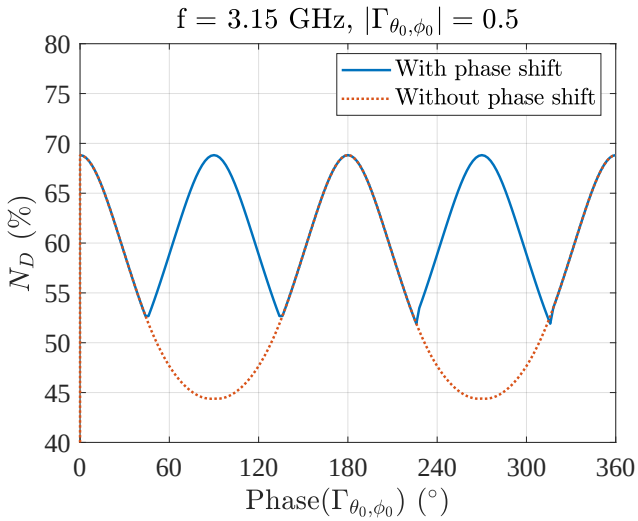

Fig. 3. Drain efficiency N_D of QB-DPA as a function of the phase of the active reflection coefficient, simulated at $f_c = 3.15$ GHz for $|\Gamma_{\theta_0,\phi_0,m}| = 0.5$.

drain efficiency as a function of the phases of the active reflection coefficient, where the drain efficiency is defined by

$$N_{m,D} = \frac{P_{m,\mathrm{OUT}}}{P_{m,\mathrm{DC}}} \tag{10}$$

where $P_m m, \mathrm{DC}$ is the power of the DC source. The efficiency varies from approximately 44% to approximately 53%.

C. Design Flow

To address the problem of improving the performance of the antenna - HPA combination in an active electronically scanning array, a stepwise approach has been followed, which is illustrated in Fig. 4. The steps are as follows:

1) The array-antenna scattering parameters and the radiated field are calculated using the commercial electromagnetic simulation tool Ansys HFSS, from which the scattering matrix and the (embedded) element patterns are extracted.
2) The scattering matrix and the embedded element patterns are both input to dedicated optimization solvers, as described in Sec. III, to calculate the optimal antenna excitations $V_{m,\mathrm{opt}}$.
3) Finally, the optimal excitations and the array scattering matrix enter the HPA analysis and design carried out in the Agilent circuit simulator ADS, in which the main design problem is to tune the HPAs input parameters to approximate as much as possible the optimized antenna excitations at their output. Finally, the obtained (approximate) excitations $\tilde{V}_{m,\mathrm{opt}}$ are used to simulate the radiation pattern of the combined array antenna and HPA.

III. Optimization Methods for the Antenna-Array Active Reflection Coefficients

In the following we describe the two optimization methods that have been employed for obtaining the optimized

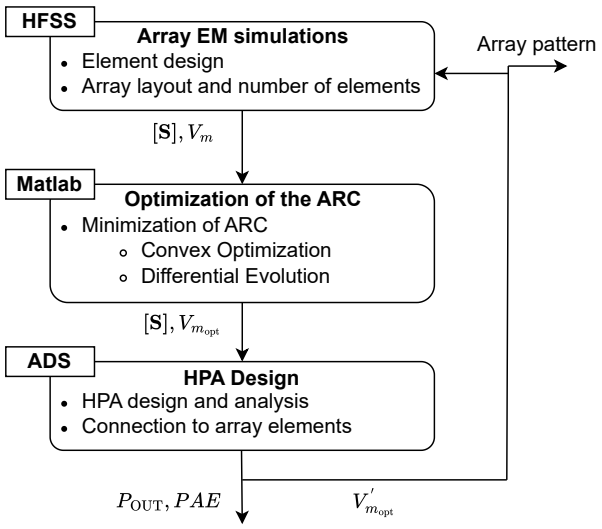

Fig. 4. Design flow for the proposed approach to improve the performance of the combined array antenna and HPA.

excitations of the antenna array. First, inspired by [15], we discuss a Differential Evolution (DE) approach for optimizing the antenna ARCs. Next, we discuss the convex relaxation introduced in our preliminary work [16], where we present some calculation details and a pseudo code of our algorithm, which are not present in [16]. Finally, we discuss how the solution of the convex problem can be used to provide an informative initial point to the DE method to further improve the obtained solution.

A. Differential Evolution Optimization

To tackle the design problem in (7), a similar approach to that of [15] has been followed, where the cost function

$$\begin{aligned}\Omega_1 = &\max\big\{-(G-G_{\text{spec}})_{\text{dB}},0\big\}\\ &+\max\big\{(SLL-SLL_{\text{spec}})_{\text{dB}},0\big\}\\ &+\max\big\{\|\mathbf{\Gamma}_{\theta_0,\phi_0}\|_\infty-|\Gamma_{\text{spec}}|,0\big\}\end{aligned}\tag{11}$$

is minimized. This cost function captures all the essential elements of (7). The softmax operation for each element makes $\Omega_1 = 0$ when all the requirements of (7) are met. Note that in contrast to (7) we have specified a desired ARC noted as Γ_{spec} in (11). This introduction equalizes the way in which the objective and constraints in (7) are dealt with in the stochastic optimization. As a by-product it also ensures that the algorithm will not search for solutions that are better than the specification.

Like other stochastic optimization methods such as genetic algorithms and particle swarm, DE does not require the objective function to be differentiable. The method can even be used for objective functions that are not continuous, but convergence may become problematic. More general, DE has few convergence guarantees like other stochastic methods.

DE optimizes (11) by maintaining a population of candidate solutions and creating new candidates by combining existing ones according to a specific protocol. Then among the new candidate solutions, the one with the best score of the objective function remains and passes through to the next iteration of the method. The performance and convergence to an optimal solution of a typical DE method mainly depends on the following parameters: the population size N_{pop}, the differential weight F, and the crossover probability CR.

For the initialization of the algorithm, one should take care of the choice of the first N_{pop} solution vectors $\mathbf{a}_{p,g}$, where p is the population indexing and g is the current generation (iteration). The vector size of $ab_{p,g}$ is the number N of antenna-array elements. As mentioned before, since the ARC minimization is aimed at high-power transmissions, it is presumed that all HPAs are in saturation, which means that there is no amplitude tuning among the antenna elements. For this reason, the solution vectors contain only phase values. The vectors in the first generation ($g = 1$) are chosen randomly from a uniform distribution within the range of $[0°, 360°)$. However, this selection is rather unspecific and the DE method may have problems to converge purely because its starting solution is too broad. Hence, it can be useful to start from a known approximate (good) solution and then apply the DE algorithm for any further improvements. To generate such a solution, one may take the optimized solution of the convex method explained in Section III-B (which will be initialized by a linear phase taper) and generate N_{pop} initial solutions for the DE method in the neighbourhood of that solution. Another approach would be to take the (globally) optimized DE population and run the convex method on every member of this population to see whether any of them can be refined. This approach has the advantage that one first looks globally in the search space where there are promising regions for optimization (without targeting convergence) and then using a local optimizer with convergence guarantees starting from each of the global solutions.

Multifrequency Cost: In (11), only the behavior at a single frequency is considered. However, in practice, requirements are set within a frequency band in the order of tens of MHz around the carrier frequency. To consider a frequency band, or better said, a range of frequencies, the objective Ω_1 can be extended to

$$\begin{aligned}\Omega_2 = &\,g\Big(\max\big\{-(G-G_{\text{spec}})_{\text{dB}},0\big\}|_{f=f_i}\Big)\\ &+g\Big(\max\big\{(SLL-SLL_{\text{spec}})_{\text{dB}},0\big\}|_{f=f_i}\Big)\\ &+g\Big(\max\big\{\|\mathbf{\Gamma}_{\theta_0,\phi_0}\|_\infty-|\Gamma_{\text{spec}}|,0\big\}|_{f=f_i}\Big)\end{aligned}\tag{12}$$

to consider multiple frequencies. Here, $g(\cdot)$ is a mapping which summarizes the performance across all frequencies. Examples for this function are $\max(\cdot)$ or $sum(\cdot)$, to name a few. In this work, we have considered the latter.

B. Convex Optimization

Next to using a general global optimization method, the just discussed DE, for the problem (7), one can also derive a convex relaxation of this problem based on semi-definite programming. Such an approach avoids the introduction of a cost function such as (11), which weights the original

objective and constraints with weight factors that need to be guessed. Also, convex optimization methods have convergence guarantees, which stochastic optimization methods generally lack. We introduced the convex relaxation of the optimization problem (7) in [16], where we also presented preliminary results of optimized ARC values and corresponding excitation coefficients and radiation patterns. Here we will briefly revisit the theory of the convex relaxation, where we present a few additional details as compared to [16] and an algorithmic description of the iterative method we devised, where in each iteration a convex optimization (also iteratively) is performed.

As detailed in [16], the convex relaxation of (7) is formulated by introducing the variable $\mathbf{A} := \mathbf{a}\mathbf{a}^{\mathrm{H}}$ and writing the optimization in terms of this variable instead of $\mathbf{a}$. This process is called lifting, which consists of creating a semi-definite matrix that allows for the construction of relaxed constraints that can be input to a convex solver.

Before we continue we should note that two of the three constraints in (7) are ratios, namely gain and sidelobe level. While ratios can be dealt with in the stochastic optimization, for the convex optimization it is necessary to formulate the constraints in terms of field magnitudes. Thus, we replace the first two constraints on gain and SLL by similar expressions as in [16, Eq. (2)], namely

$$\|\mathbf{E}(\theta_0, \phi_0; \mathbf{a})\|_2 \geq g_{\min} \tag{13}$$

and

$$\max_{(\theta,\phi)\in\Theta} \|\mathbf{E}(\theta, \phi; \mathbf{a})\|_2 \leq s_{\max} \tag{14}$$

Then, as derived in [16] the constraints in terms of $\mathbf{A}$ are given by

$$\mathrm{C1}: \quad \mathbf{v}_{\theta_0,\phi_0}^{\top} \mathbf{A} \mathbf{v}_{\theta_0,\phi_0}^{*} \geq g_{\min}^2 \tag{15}$$

$$C2: \quad \|\mathrm{diag}(\mathbf{V}_{\Theta}^{\top} \mathbf{A} \mathbf{V}_{\Theta})\|_{\infty} \leq s_{\max}^2 \tag{16}$$

$$C3: \mathrm{trace}(\mathbf{A}) = 1 \tag{17}$$

where $\mathbf{v}_{\theta_0,\phi_0}$ is the co-polarized (electric-field) component of the embedded element patterns at the direction (θ_0, ϕ_0), and $\mathbf{V}_{\Theta} := [(\mathbf{v}_{\theta_1,\phi_0}, \ldots, \mathbf{v}_{\theta_K,\phi_K}]$ are the co-polarized components of the embedded element patterns at the directions $\{(\theta_1, \phi_1), \ldots, (\theta_K, \phi_K)\} =: \Theta$. These three constraints should be supplemented by the constraint $\mathrm{rank}(\mathbf{A}) = 1$, which represents the matrix $\mathbf{A}$ being constructed from a single vector.

It should be noted that one could introduce also a constraint on the cross-polarized field component. In [16] we have only verified a posteriori the cross-polarization level, which is of the same order of magnitude for a scan towards broadside, around -35 dB to -40 dB in an array of $0.455\ \lambda$ dipoles and of half wavelength spacing. In contrast, for 50° of scan, the cross-polarization is fairly high (maximum around -10 dB), since no wide-angle impedance matching is performed. In this paper we will not further investigate suppressing high cross-polarization components.

A weakness of the formulation of constraint C2, which is not described in [16], is that a standard implementation will calculate first $\mathbf{V}_{\Theta}^{\top} \mathbf{A} \mathbf{V}_{\Theta}$ and then take the diagonal, which means that a matrix of size $N_{SLL} \times N_{SLL}$ is stored in RAM. If the sidelobe region is densely sampled, this matrix can be of prohibitively large size, while only the diagonal is needed. For this reason, we employ a second identity, namely $\mathrm{diag}(\mathbf{C}\mathbf{B}^{\top}) = (\mathbf{C} \odot \mathbf{B})\, \mathbf{1}$, where $\mathbf{1}$ is a vector of ones and $\odot$ is the point-wise (Hadamard) product. Applying this identity with $\mathbf{C} = \mathbf{V}_{\Theta}^{\top}$ and $\mathbf{B} = \mathbf{V}_{\Theta}^{\mathrm{H}} \mathbf{A}^{\top}$, we obtain

$$\mathrm{diag}(\mathbf{V}_{\Theta}^{\top} \mathbf{A} \mathbf{V}_{\Theta}^{*}) = \left(\mathbf{V}_{\Theta}^{\top} \odot \mathbf{V}_{\Theta}^{\mathrm{H}} \mathbf{A}^{\top}\right) \mathbf{1}_{N\times 1} \tag{18}$$

The evaluation of the right-hand side requires only the storage of the matrix $\mathbf{V}_{\Theta}$ in RAM, which has size $N \times N_{SLL}$. If the angular region is the complete hemisphere except for a small mainlobe region, N_{SLL} will be significantly larger than the number of antenna elements N to sample sufficiently well the far-field pattern. Therefore we replace the constraint by

$$C2: \quad \|\left(\mathbf{V}_{\Theta}^{\top} \odot \mathbf{V}_{\Theta}^{\mathrm{H}} \mathbf{A}^{\top}\right) \mathbf{1}_{N\times 1}\|_{\infty} \leq SLL_{\mathrm{spec}} \tag{19}$$

To obtain an objective-function expression in terms of $\mathbf{A}$, the expression $\|\mathbf{\Gamma}\|_{\infty}$ is replaced by $\||\mathbf{\Gamma}|^{\odot 2}\|_{\infty}$, where $^{\odot 2}$ is component-wise squaring,

$$\||\mathbf{\Gamma}|^{\odot 2}\|_{\infty} = \|\mathrm{diag}(\mathbf{A}^{\odot -1} \odot \mathbf{S}\mathbf{A}\mathbf{S}^{\mathrm{H}})\|_{\infty} \tag{20}$$

see [16, Eq. (9), (10)] for details. But, as noted in [16], the optimization problem defined by this objective and the four constraints is still non-convex for two reasons: 1) the dependency of the objective function on a self product of $\mathbf{A}$ and 2) the rank constraint. The solution to the first problem is to replace the inverse of $\mathbf{A}$ in (20) by the matrix $\mathbf{D}_k := \mathrm{diag}((\mathbf{a}_k^{\odot -1})(\mathbf{a}_k^{\mathrm{H}})^{\odot -1}))$ and consider $\mathbf{D}_k$ fixed in each iteration of an iterative procedure where a convex problem is solved per iteration. The solution to the second problem is to replace the rank constraint by a constraint that requires $\mathbf{A}$ to stay close to the rank-one matrix $\mathbf{D}_k$. Then we get the following optimization problem

$$\begin{aligned} \mathbf{A}_{k+1} := \underset{\mathbf{A}\in\mathbb{S}_+^{M\times M}}{\arg\min} \quad & \|\mathrm{diag}(\mathbf{D}_k \odot \mathbf{S}\mathbf{A}\mathbf{S}^{\mathrm{H}})\|_{\infty} \\ \text{s.t.} \quad & \mathbf{v}_{\theta_0,\phi_0}^{\top} \mathbf{A} \mathbf{v}_{\theta_0,\phi_0}^{*} \geq G_{spec} \\ & \|\left(\mathbf{V}_{\Theta}^{\top} \odot \mathbf{V}_{\Theta}^{\mathrm{H}} \mathbf{A}^{\top}\right) \mathbf{1}_{N\times 1}\|_{\infty} \leq SLL_{spec} \\ & \mathrm{trace}(\mathbf{A}) = 1 \\ & \|\mathbf{A} \odot \mathbf{D}_k - \mathbf{1}_{N\times N}\|_F < \varepsilon_{AD} \end{aligned} \tag{21}$$

where $\mathbb{S}_+$ denotes the set of positive-semidefinite (complex) matrices, $\|\cdot\|_F$ is the Frobenius norm, $\mathbf{1}_{N\times N}$ is a $N \times N$ matrix of ones, and ε_{AD} is a tuning parameter. Also, the iterate $\mathbf{a}_k$ is obtained by performing a rank-one approximation of the optimization solution, i.e., $\mathbf{a}_k$ is the eigenvector of $\mathbf{A}_k$ with the largest eigenvalue. The eigenvector $\mathbf{a}_k$ should be normalized to satisfy the norm constraint. Also, since all HPAs are assumed to be in saturation, and thus no amplitude tuning is possible, the eigenvector $\mathbf{a}_k$ is replaced by $\mathrm{diag}(|\mathbf{a}_k|^{\odot -1})\mathbf{a}_k$ such that only the phase information of each component is preserved. As problem (21) is a semi-definite program, when $\mathbf{D}_k$ is fixed, it can be solved with efficient off-the-shelf convex solvers. Problem (21) is solved several times up to a number of iterations or up to a convergence criterion is reached. The initial vector of excitation coefficients can be set to e.g. the nominal beamformer for the scan direction θ_0, but one can of

Algorithm 1 Iterative Optimization of ARCs

Require: $g_{\min}$: lower bound on E-field magnitude in scan direction,
$s_{\max}$: upper bound on E-field magnitude in sidelobe region,
Θ : angles in the sidelobe-region, (θ_0, ϕ_0) : scan direction,
$\mathbf{a}_{\text{init}}$: vector with initial excitations,
$\mathbf{\Gamma}_{\text{init}}$: vector with initial ARC values,
$\Gamma_{\max}$: threshold on maximum ARC magnitude,
$k_{\max}$: maximum number of iterations,
ε_{AD} : rank-one threshold

Ensure: $k \leftarrow 0$, $\mathbf{a}_0 \leftarrow \mathbf{a}_{\text{init}}$, $\mathbf{\Gamma}_0 \leftarrow \mathbf{\Gamma}_{\text{init}}$
  while $\mathbf{\Gamma}_k \geq \Gamma_{\max}$ & $k < k_{\max}$ **do**
    $\mathbf{D}_k = \text{diag}((\mathbf{a}_k^{\odot -1})(\mathbf{a}_k^{\text{H}})^{\odot -1}))$
    $\mathbf{A}_{k+1} \leftarrow$ Solve (21)
    $\mathbf{a}_{k+1} \leftarrow \text{eigs}(\mathbf{A}_{k+1}, 1)$
    $\mathbf{a}_{k+1} \leftarrow \text{diag}(|\mathbf{a}_{k+1}|^{\odot -1})\mathbf{a}_{k+1}$
    $\mathbf{\Gamma}_{k+1} \leftarrow \text{diag}(\mathbf{a}_{k+1}^{\odot -1})\mathbf{S}\mathbf{a}_{k+1}$
    $k \leftarrow k+1$, $\mathbf{a}_k \leftarrow \mathbf{a}_{k+1}$, $\mathbf{\Gamma}_k \leftarrow \mathbf{\Gamma}_{k+1}$
  end while
  return $\mathbf{a}_k$, $\mathbf{\Gamma}_k$

course use another initial vector, for example one obtained from a previous optimization. The optimization procedure, with only one tuning parameter (ε_{AD}), is summarized by the pseudo-code Algorithm 1.

IV. Numerical Results

A. Simulation Setup

As a test geometry, we consider an 8x8 dipole array, similar to [15] and [16]. The spacing among the elements is half wavelength at 3.15 GHz and the dipole length and radius are equal to 0.455λ and 0.01λ, respectively at the same frequency. Fig. 5 shows the layout of the dipole array and the port indexing. We analyze this structure using the Finite Element Method (FEM) solver in HFSS to calculate the scattering parameters and the embedded element patterns. The spherical components of the electric-field E_ϕ and E_θ are exported, using the classical definition of a spherical coordinate system, where θ is the angle with respect to the z-axis and ϕ the angle in the xy-plane with respect to the $x$axis. Then, a classical transformation to uv-coordinates is used, where $u = \sin\theta\cos\phi$ and $v = \sin\theta\sin\phi$. For the optimization, the co- and cross-polarized components of the electric fields are used, based on the Ludwig-3 definition [26].

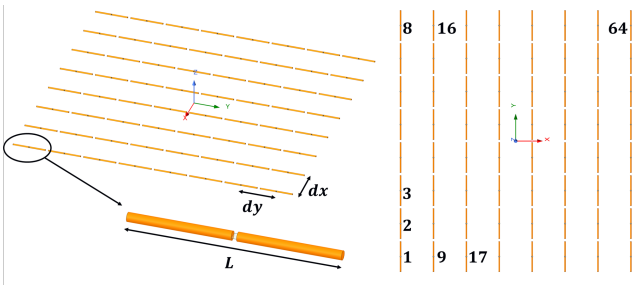

Fig. 5. 8x8 dipole array layout with its coordinate system and port indexing

B. Single Frequency Optimization

For the results of the dipole array, both the (iterative) convex method based on CVX and the DE algorithm are considered. Both optimization methods have been applied to the simulated data at the central frequency 3.15 GHz, minimizing the objective function in (11) by the DE method and carrying out the iterative scheme (21) of the (iterative) convex method. For the DE method the maximum number of iterations is set to 1000 with parameters $F = 0.8$, $N_{\text{pop}} = 320$, and $CR = 0.9$. For the iterative convex method, the maximum number of iterations is 40 and the tuning parameter ε_{AD} is set equal to 1. The optimized results are compared with the case where the antenna elements use a linear phase excitation, i.e., the typical beam scanning excitation for pointing towards direction (θ_0, ϕ_0). For simplicity, this case will be referred to as "Linear". The DE method is initialized in two different ways: (i) global initialization, where all the antenna elements start with a random phase within the range $[0°, 360°)$ and (ii) local initialization using as a reference the CVX solution with a maximum random variation of $20°$ per element. The target values for both optimizers are set equal to -10dB for the maximum ARC, -13dB for the SLL and a constraint of 0.2dB drop of the realized gain with respect to the linear case.

In Fig. 6(a) and Fig. 6(b) the magnitude of the ARCs per antenna element at the central frequency 3.15 GHz, for two different scan directions: broadside and $(\theta_0, \phi_0) = (50°, 0°)$. Each curve corresponds to a different optimization approach, including also the linear phase progression (solid blue). The dashed black line shows the Γ_{spec}, which is -10 dB for both cases. In Fig. 7 and Fig. 8 the realized gain patterns for the same cases in different azimuth or elevation planes are shown. More specifically, for broadside, the azimuth plane ($\phi = 0°$ and the elevation plane $\phi = 90°$) are depicted as a function of the angle θ, while for the other case the circular "plane" $\theta = 50°$ and the azimuth plane $\phi = 0°$ are presented, respectively.

All methods show a promising performance regarding the minimization of the highest ARC of the linear phase progression, with an improvement of at least 9% – 14% as compared to that case. The DE with a fully random initial phase population (indicated as DE (global)) slightly outperforms the iterative convex method (indicates as CVX). A rather significant improvement of that result is obtained when the DE method is initialized by a more focused initial population derived from the result of the convex method (indicated as DE (onCVX)). Then, the improvement as compared to the result for the linear phase progression is approximately 23%.

Both optimization methods show a minor loss of the realized gain as compared to the linear case, see the insets of Figs. 7 and 8. More importantly, in some cases, various methods show a beam squint. For scanning to broadside, such a beam squint is only present in the DE results (both global and onCVX) and limited to the elevation plane. In the azimuth plane, no beam squint occurs. For scanning to $(\theta_0, \phi_0) = (50°, 0°)$, no beam squint seems to occur in the circular "plane", but a quite strong squint occurs in the azimuth plane, as the inset of Fig. 8(b) shows. The biggest beam squints occur for the two DE methods and are approximately $2°$. The iterative convex

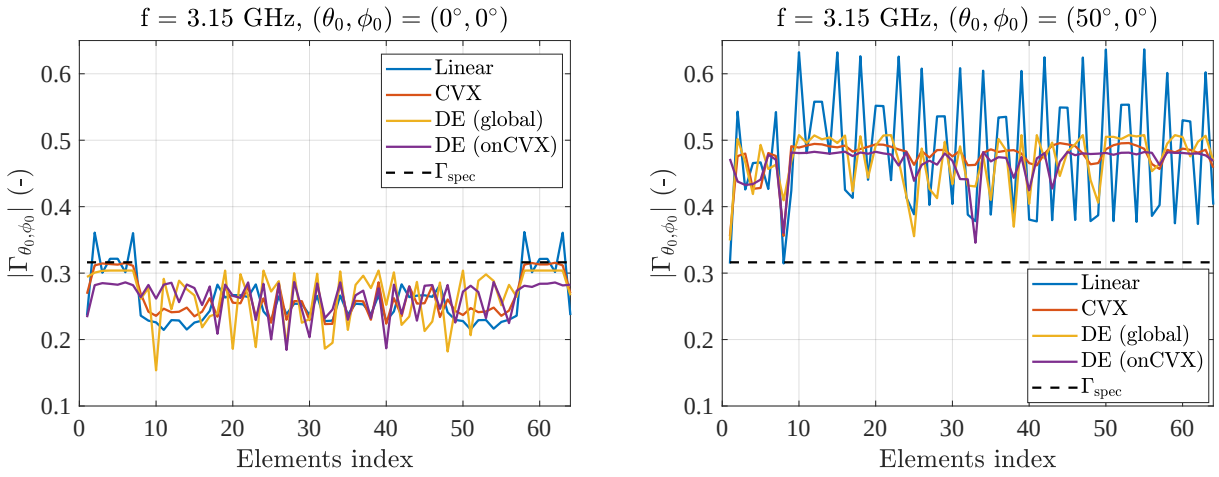

(a) (b)

Fig. 6. Magnitude of the ARCs per antenna element at $f_c = 3.15$ GHz, both for the linear and the different optimized phase excitations. (a) Scan to broadside or $(\theta_0, \phi_0) = (0°, 0°)$, (b) Scan to $(\theta_0, \phi_0) = (50°, 0°)$.

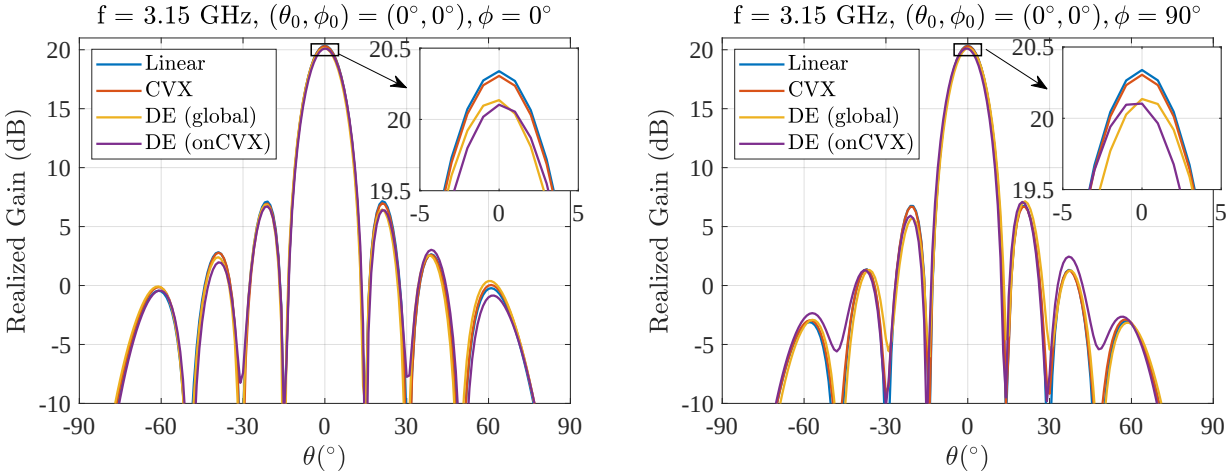

(a) (b)

Fig. 7. Realized gain patterns for the linear phase progression and the different optimization approaches when scanning to broadside at $f_c = 3.15$ GHz. (a) Azimuth plane $\phi = 0°$. (b) Elevation plane $\phi = 90°$.

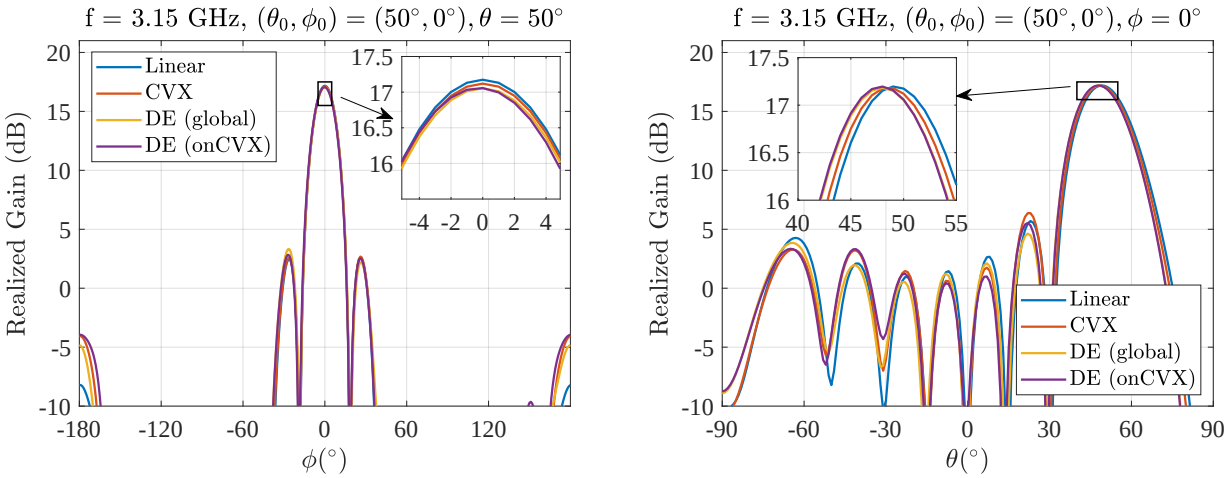

(a) (b)

Fig. 8. Realized gain patterns for the linear phase progression and the different optimization approaches when scanning to $(\theta_0, \phi_0) = (50°, 0°)$ at $f_c = 3.15$ GHz. (a) Circular "plane" $\theta = 50°$. (b) Azimuth plane $\phi = 0°$.

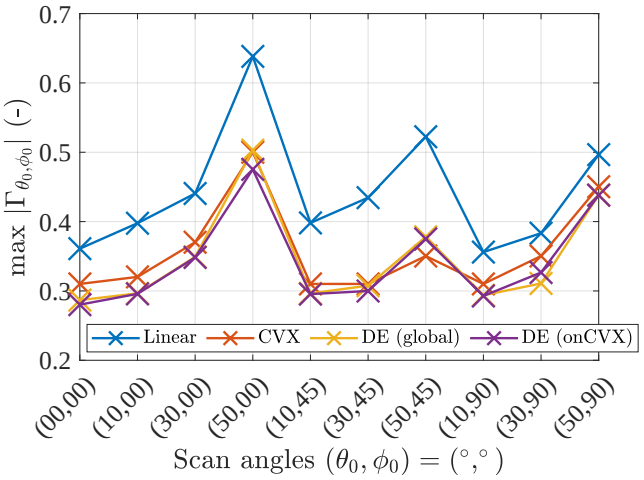

Fig. 9. Maximum ARC versus scan direction for the 8 × 8 dipole array excited at 3.15 GHz, as obtained by the four different methods.

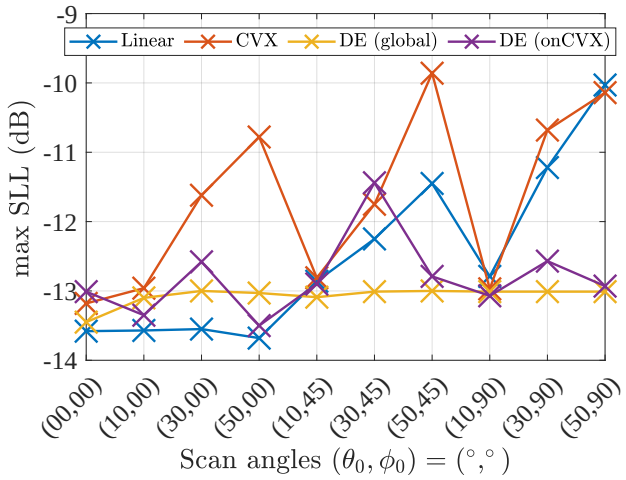

Fig. 10. Maximum SLL versus scan direction for the 8 × 8 dipole array excited at 3.15 GHz, as obtained by the four different methods.

method and the linear phase progression have slightly smaller beam squints.

When it comes to the maximum SLL, there are minor differences in the azimuth and elevations planes when scanning to broadside. Also, when scanning to $(\theta_0, \phi_0) = (50°, 0°)$, there are hardly differences in the circular "plane" $\theta = 50°$. However, in the azimuth plane, the global DE method outperforms the other two methods (and the linear phase progression).

As a next step, we will determine the maximum ARC, the maximum SLL, and the gain for 10 different scan directions. The gain and maximum SLL will be determined from the complete 2D radiation patterns. To determine the maximum SLL, the Matlab function findpeaksn.m [27] is used which can detect all the local maxima of the 2D radiation pattern. Figs. 9, 10 and 11 show the maximum ARC, maximum SLL, and realized gain, respectively, for a broadside scan and for scanning to $\theta = 10°, 30°, 50°$ in the azimuth plane $\phi = 0°$, the diagonal plane $\phi = 45°$, and the elevation plane $\theta = 90°$.

In the maximum ARC plot of Fig. 9, we observe that the three optimization methods indeed reduce the maximum ARC for all ten scan directions. Also, the difference between the linear phase progression and any of the three optimization methods is significantly bigger than the differences among the three optimization methods. At least from an ARC perspective there is no clear outstanding method, though the two DE methods perform slightly better than the iterative convex method.

In the maximum SLL plot of Fig. 10 we observe clearly that the global DE method provides the most uniform maximum SLL, which is around -13 dB for all ten scan directions. The iterative convex method shows the most fluctuating maximum SLL followed by the linear phase progression. The DE method initialized by the iterative convex method (labeled DE (onCVX)) shows a weakly fluctuating maximum SLL except for scanning to $\theta = 30°$ in the diagonal plane.

Finally, the realized gain plot of Fig. 11 shows than the fluctuation of the realized gain over the different scan directions is way bigger, around 3 dB, than the differences among the four different methods, which are in the order of a few tenths of dB.

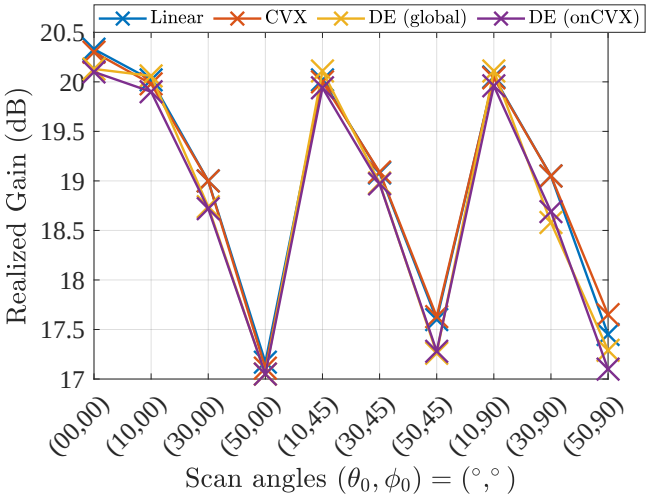

Fig. 11. Gain versus scan direction for the 8 × 8 dipole array excited at 3.15 GHz, as obtained by the four different methods.

In conclusion we can say that the maximum ARC and the realized gain do not show a preference for any of the three optimization methods, except that the two DE methods outperform the iterative convex method slightly. When it comes to maximum SLL, it seems that the global DE method is the preferred choice.

C. Multiple Frequency Optimization

To treat multiple frequencies at once, we can use the multi-frequency optimization described in Sec. III-A for the DE method. The main goal here is to compare the maximum ARC, the maximum SLL, and the realized gain when the global DE method is used for (i) minimizing (11) at a single frequency and (ii) minimizing (12) at multiple frequencies. For the multiple frequencies, we set $M = 3$, where $f_1 = 3.1$ GHz, $f_2 = 3.15$ GHz and $f_3 = 3.2$ GHz.

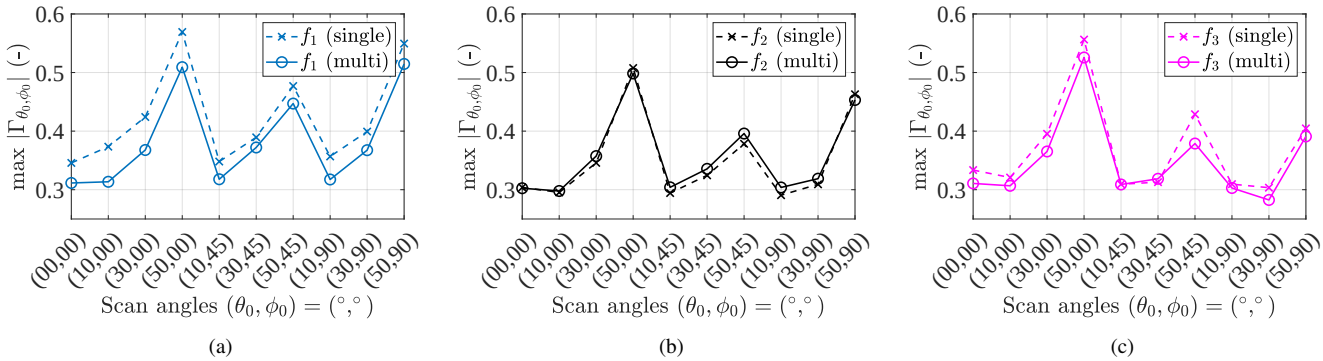

Fig. 12. Magnitude of maximum ARC versus scan direction for three frequencies and two optimization types when applying the global DE method. The dashed line corresponds to single-frequency optimization, while the solid line corresponds to multi-frequency optimization. (a) $f_1 = 3.1$ GHz. (b) $f_2 = 3.15$ GHz. (c) $f_3 = 3.2$ GHz.

Using the same DE parameters and the same maximum number of iterations as in the single frequency optimization, Fig. 12, Fig. 13 and Fig. 14 show the maximum ARCs, the maximum SLLs and the realized-gain drops, as compared to the realized gains of the linear phase progression. For the maximum ARC in Fig. 12 we observe that the differences among various scan directions is significantly bigger than the differences between the single and multi-frequency optimization at a specific scan direction. For 3.1 GHz and 3.2 GHz, the multi-frequency optimization outperforms the single-frequency optimization, with the biggest differences of 0.04 to 0.05 (linear ARC scale) occuring in the azimuth plane $\phi = 0^\circ$ at 3.1 GHz. At 3.15 GHz, there is hardly a difference between the results of the single and multi-frequency optimization.

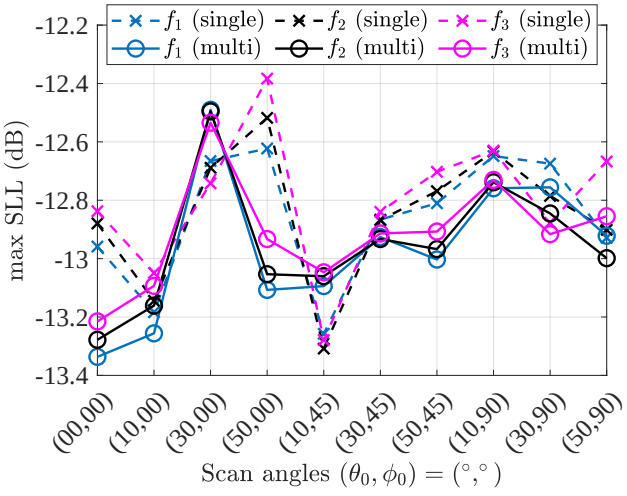

Fig. 13. Maximum SLL versus scan direction for three frequencies and two optimization types when applying the global DE method. The dashed line corresponds to single-frequency optimization, while the solid line corresponds to multi-frequency optimization.

In the maximum SLL plot of Fig. 13, multi-frequency optimization seems to work generally better than or equal to single-frequency optimization resulting in 0.5 to 1 dB lower maximum SLL. Only for two scan directions, $(\theta_0, \phi_0) = (30^\circ, 0^\circ)$ and $(\theta_0, \phi_0) = (10^\circ, 45^\circ)$, single-frequency optimization outperforms multi-frequency optimization. Finally, the gain-drop plot of Fig. 14 shows that single and multi-frequency optimization lead to gain drops of 0 to 0.6 dB as compared to the gain of the linear phase progression, with no clear verdict of which optimization results in a lower gain drop. Thus, in conclusion, multi-frequency optimization leads generally to a lower or equal maximum ARC value and to a lower or equal maximum SLL as compared to single-frequency optimization. For realized gain, there is no clear verdict which of the two optimization types is the best.

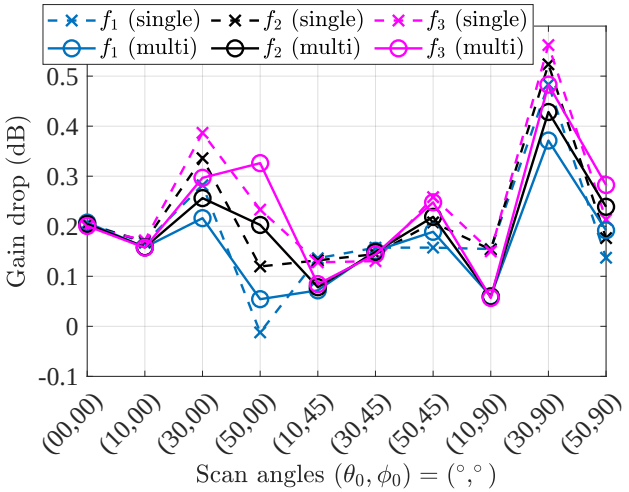

Fig. 14. Realized gain drop (as compared to the gain of the linear phase progression) versus scan direction for three frequencies and two optimization types when applying the global DE method. The dashed line corresponds to single-frequency optimization, while the solid line corresponds to multi-frequency optimization.

D. Amplitude and Phase Errors

In this subsection, we analyze the effect of amplitude and phase errors caused by the non-ideal active electronics. Specifically, a maximum error of 0.25 dB can be expected in the measurements of the output power of the amplifiers due to process variations. To implement this maximum power value as voltage amplitude errors in the antenna ports, random voltage values have been selected for the antenna ports according

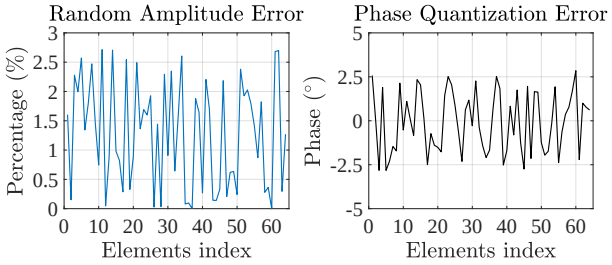

Fig. 15. (Left) Amplitude errors over the antenna ports as calculated in (22) for scan direction $(\theta_0, \phi_0) = (50°, 0°)$ at 3.15 GHz with excitation coefficients obtained by the global DE method. (Right) Corresponding phase errors on the antenna ports due to phase quantization that a 6-bit digital phase shifter induces.

to a uniform distribution on $[0.97, 1]$. As for the phase, we consider quantization errors which arise from the use of a 6-bit digital phase shifter for each antenna port. Consequently, the phase shifter has $2^6 = 64$ different phase values, which are uniformly distributed in the range $[0°, 360°)$.

Fig. 15 shows the amplitude and phase errors of the port excitations when scanning to $(\theta_0, \phi_0) = (50°, 45°)$ at the central frequency $f_c = 3.15$ GHz. The excitation coefficients are those obtained by the global DE method affected by one specific realization of the random amplitude and phase errors, as described in the previous paragraph. Also, the amplitude error in the figure is defined by

$$error = \Big(\frac{|\mathbf{1}_{N\times 1} - \mathbf{a}_{\rm er}|}{\mathbf{1}_{N\times 1}}\Big) \cdot 100\% \qquad (22)$$

where $\mathbf{1}_{N\times 1}$ is a vector of ones representing a unit amplitude for each element, $\mathbf{a}_{\rm er}$ is the amplitude distribution over the antenna ports, and $|\cdot|$ is the componentwise magnitude of a vector. The presented amplitude and phase errors are input to the calculated ARC values shown in Fig. 16. Scan direction and frequency are of course the same. As the figure clearly shows, the impact of the random errors on the ARCs of the antenna ports is minor.

E. HPA Performance in Combination with Antenna

An ideal QB-DPA has been combined with the 8x8 dipole antenna and simulated in ADS. For this test, it is assumed that for each scan direction the active reflection coefficients of the antenna ports are known and used as input parameter of the amplifiers. The simulation results show a low error between the reflection coefficients that are known from the antenna-only simulations and the ones obtained from the ADS simulation. The error is less than 6% for $|\Gamma_{\theta_0,\phi_0,m}| > 0.1$.

The amplifier performance has been studied in combination with the previously discussed 8×8 dipole array. The results of the 64 amplifiers that are connected to the antenna elements are depicted in Fig. 17. Three cases are compared:

- optimized antenna-element excitations and compensated amplifier,
- linear phase progression as antenna-element excitations and compensated amplifier,
- Linear phase progression as antenna-element excitations and uncompensated amplifier.

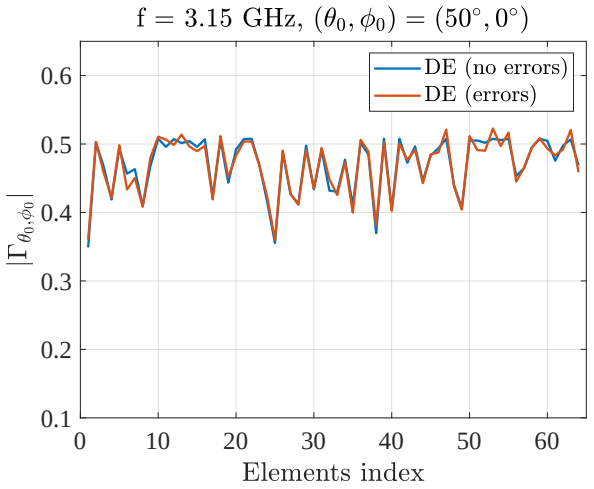

Fig. 16. Magnitude of the ARCs per antenna element when scanning to $(\theta_0, \phi_0) = (50°, 0°)$ at 3.15 GHz with port excitations obtained by the global DE method. Blue curve: no amplitude and phase errors on the port excitations. Red curve: including amplitude and phase errors.

For the case that the amplifier is uncompensated, a 50 Ω load at its output is assumed. In Fig. 17 we observe clearly that the compensation of the amplifiers is necessary to improve the output power and the power-aided efficiency (PAE), and to keep the dissipated power limited. The compensated case has approximately two to ten times the output power of the uncompensated case, a few tens of percents more in PAE, and two to ten times lower dissipated power. As for the linear versus optimized antenna-element excitations, they lead to approximately the same output power, PAE, and dissipated power, except that the optimization improves the outliers of the linear phase progression significantly. Specifically, consider for example the lowest four PAE values of the case "Comp PA + linear excitations" (red pluses) presented in the middle plot of Fig. 17. They correspond to the four highest active reflection coefficients. The PAE values are greatly improved by the optimization by 10% to 15% (from red pluses to blue asterisks) and the corresponding active reflection coefficients reduce by 0.1 to 0.2. Analogously, the lowest two output-power values are increased by about 10 W and the highest four or five dissipated-power values are lowered by by about 10 W.

Fig. 18 shows the 2D normalized radiation patterns expressed in uv-coordinates at $f_c = 3.15$ GHz with scan direction $(\theta_0, \phi_0) = (50°, 45°)$ for the three amplifier plus antenna-array designs. Fig. 19 shows the realized gain patterns for two different planes (circular "plane" $\theta = 50°$ and diagonal plane $\phi = 45°$), in which the maximum gain occurs. Both figures show that the sidelobe level is hardly affected by the optimization and compensation. Secondly, gain losses are smaller than 0.25 dB as the insets of Fig. 19 show. Thirdly, the compensation and optimization show an additional beam squint of approximately $0.1°$ to $0.2°$ as compared to the uncompensated case with linear phase progression as antenna-elements' excitations. This additional squint is small compared to the beam squint occuring for oblique scanning of the

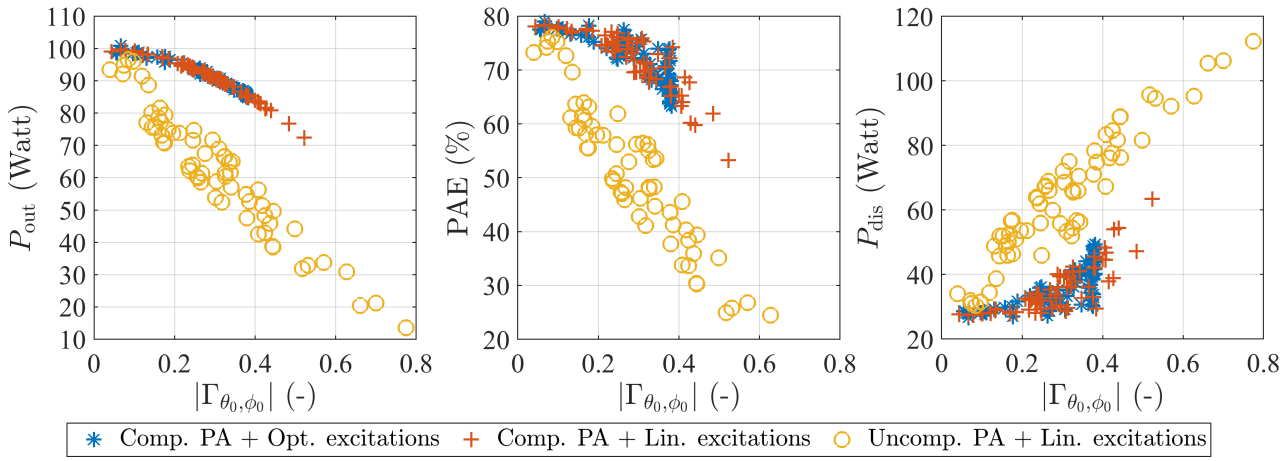

Fig. 17. Performance of the 64 amplifiers in combination with the 8×8 dipole array for three different excitation cases simulated at $f_c = 3.15$ GHz with scan direction $(\theta_0, \phi_0) = (50°, 45°)$. (Left) Optimized antenna-element excitations and compensated amplifier. (Middle) Linear phase progression as antenna-element excitations and compensated amplifier. (Right) Linear phase progression as antenna-element excitations and uncompensated amplifier.

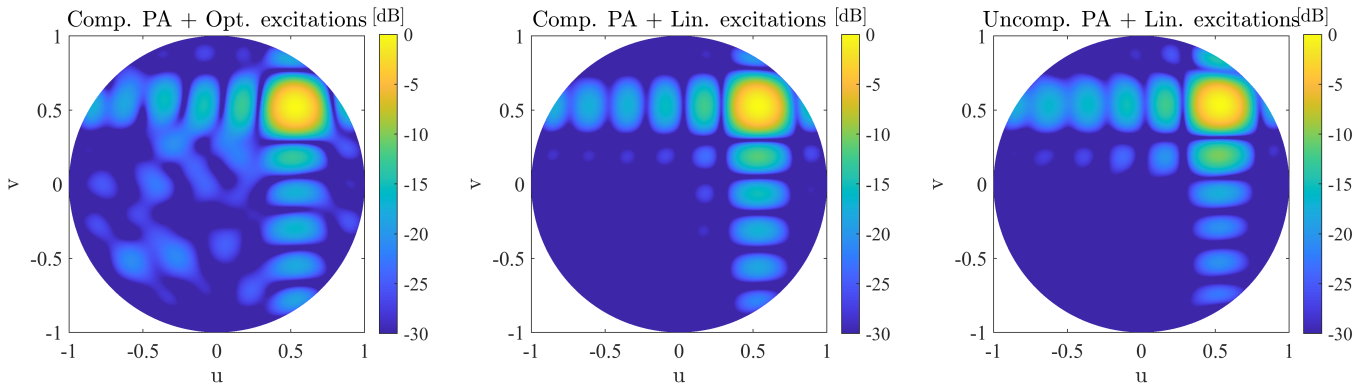

Fig. 18. Normalized radiation patterns of the 8×8 dipole array, expressed in uv-coordinates, for three different excitation cases simulated at $f_c = 3.15$ GHz with scan direction $(\theta_0, \phi_0) = (50°, 45°)$. The excitation cases are the same as in Fig. 17.

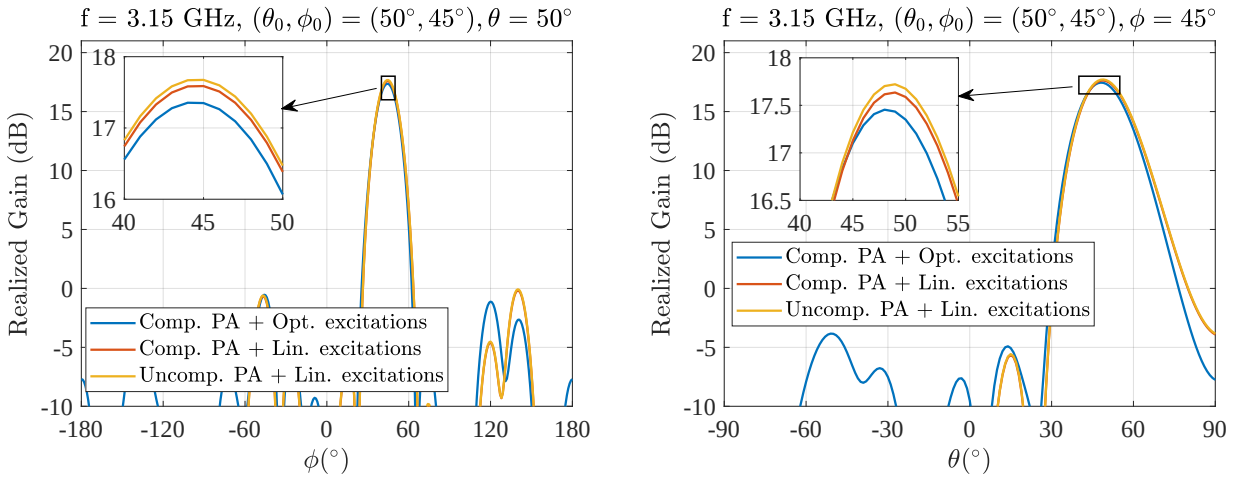

(a) (b)

Fig. 19. Realized gain patterns for three different excitation cases when scanning to $(\theta_0, \phi_0) = (50°, 45°)$ at $f_c = 3.15$ GHz. (a) Circular "plane" $\theta = 50°$. (b) Diagonal plane $\phi = 45°$. The excitation cases are the same as in Fig. 17.

order of 1°. For the specific case of scanning to $(\theta_0, \phi_0) = (50^\circ, 45^\circ)$, the "oblique" beam squint and the additional beam squint by compensation and optimization occur primarily in the diagonal plane as the insets of Fig. 19 show.

V. Conclusions

This paper focuses on enhancing the output power and sensitivity of an AESA by i) reducing the active reflection coefficients (ARCs) at the antenna ports by the use of dedicated optimization methods to determine optimal antenna-element excitations and ii) improving the active impedance matching at the interface between the antenna elements and the power amplifiers. For the minimization of the active reflection coefficients, three optimization methods have been used successfully: 1) a dedicated iterative convex method developed in this paper, 2) a global differential evolution method where global refers to the fully random initialization, and 3) a local differential evolution method where local refers to the initialization by agents that are weakly perturbed variants of a solution of the iterative convex method. In all three cases, only the phases of the antenna excitation coefficients are optimized, since the focus is on a Radar-related application where power amplifiers are operated in saturation. All three methods show clearly the improvements in terms of reduced ARC values, while reasonably maintaining SLL and gain. Especially the third method of local differential evolution is very promising for achieving active reflection coefficients as low as possible. Another potential improvement could be obtained by formulating a multi-frequency objective for the differential-evolution optimization, which works better than or equally good as its single-frequency counterpart. Finally, random amplitude errors, associated to manufacturing tolerances, and quantization phase errors show minor impact on the minimized active reflection coefficients.

With respect to the power-amplifier side of our work, we investigated an architecture able to compensate for the variation of the ARC based on a QB-DPA. The QB-DPA can control the output power and reduce the variation of the power-aided efficiency with the load impedance. The performance of the power amplifiers connected to the array antenna equipped with the optimal excitations was jointly evaluated. The biggest improvement is achieved by compensation at the power amplifiers for the active-reflection coefficients of the antenna elements: two to ten times higher output powers, a few tens of percents higher PAEs, and two to ten times lower dissipated powers. If one also replaces the linear phase progression of the excitation coefficients of the antenna elements by dedicated optimized excitation coefficients further improvements of about 10 W output power per antenna element and 10% in PAE per antenna element are achieved.

Acknowledgments

We would like to express our gratitude to Alessandro Garufo for his inputs and useful discussions during this study.

References

[1] S. Kingsley and S. Quegan,*Understanding Radar Systems*, McGraw-Hill, 1992.

[2] R. J. Mailloux, *Phased Array Antenna Handbook*, Artech House, Boston and London, 1994.

[3] C. Yepes, E. Gandini, S. Monni, A. Neto, F. E. van Vliet and D. Cavallo, "Analysis of Tilted Dipole Arrays: Impedance and Radiation Properties," *IEEE Trans. Antennas Propag.*, vol. 68, no. 1, pp. 254-265, Jan. 2020.

[4] E. Gandini, F. Silvestri, A. Benini, G. Gerini, E. Martini, S. Maci, M. C. Viganò, G. Toso and S. Monni, "A dielectric dome antenna with reduced profile and wide scanning capability," *IEEE Trans. Antennas Propag.*, vol. 69, no. 2, pp. 747-759, Feb. 2021.

[5] R. D. Palmer, M. B. Yeary, D. Schvartzman, J. L. Salazar-Cerreno, C. Fulton, M. McCord, B. Cheong, D. Bodine, P. Kirstetter, H. Sigmarsson, T. Yu, D. Zrnic, R. Kelley, J. Meier and M. Herndon, "Horus–A fully digital polarimetric phased array radar for next-generation weather observations," *IEEE Trans. Radar Systems*, vol. 1, pp. 96-117, May 2023.

[6] C. Fulton, M. Yeary, D. Thompson, J. Lake and A. Mitchell, "Digital phased Arrays: challenges and opportunities," *Proc. IEEE*, vol. 104, no. 3, March 2016, pp. 487-503.

[7] J. S. Herd and M. D. Conway, "The evolution to modern phased array architectures," *Proc. IEEE*, vol. 104, no. 3, 2015, pp. 519–529.

[8] E. Holzman, "On removing circulator and isolators from active electronic scanned array front ends," *IEEE Int. Symp. Phased Array Systems and Tech.*, Boston, USA, 15-18 Oct. 2024.

[9] A. P. de Hek, G. van der Bent, F. E. van Vliet, "400-Watt S-band power amplifier MMIC," in *Proc. 16th Eur. Microwave Integrated Circuits Conf. (EuMIC)*, London, UK, 3-4 April 2022.

[10] A. Garufo, E. M. Suijker, D. C. A. Ribeiro, C. Trampuz, S. Monni, "Characterization of all-metal multi-feed antenna for high power applications," in *Proc. 18th Eur. Conf. Antennas Propag. (EuCAP)*, Glasgow, UK, 17-22 March 2024 [Online: https://repository.tno.nl/SingleDoc?docId=70950].

[11] D. Cavallo, W. H. Syed, and A. Neto, "Connected-slot array with artificial dielectrics: a 6 to 15 GHz dual-pol wide-scan prototype," *IEEE Trans. Antennas Propag.*, vol. 66, no. 6, Jun. 2018, pp. 3201–3206.

[12] A. van Bezooijen et al., "RF-MEMS based adaptive antenna matching module," *IEEE Radio Freq. Intergr. Circuits (RFIC) Symposium*, Honolulu, HI, USA, 2007.

[13] P. W. Hannan, D. S. Lerner, and G. H. Knittel, "Impedance matching a phase-array antenna over wide scan angles by connecting circuits," *IEEE Trans. Antennas and Propag.*, Vol. 13, no. 1, Jan. 1965 pp. 28-34.

[14] S. M. Duffy, G. A. Brigham and J. S. Herd, "Integrated Compensation Network for Low Mutual Coupling of Planar Microstrip Antenna Arrays," *IEEE Antennas and Propag. Soc. Int. Symp.*, Honolulu, USA, 9-15 June 2007.

[15] H.-T. Chou, R.-Z. Wu, M. O. Akinsolu, Y. Liu and B. Liu, "Radiation optimization for phased arrays of antennas incorporating the constraints of active reflection coefficients," *IEEE Trans. Antennas Propag.*, vol. 70, no. 12, Dec. 2022, pp. 11707–11717.

[16] D. Bekers, M. Coutiño Minguez, C. Stefopoulos and S. Monni, "Convex minimization of active reflection coefficients in antenna arrays with radiation pattern constraints," *IEEE Int. Symp. Phased Array Systems and Technology*, 15-18 Oct. 2024, Boston, USA.

[17] J. Hou, H. Fan, Y. Ding and G. Goussetis, "Orthogonal vector approach for reducing loadpulling effect in MIMO transmitters," *Proc. 54th Eur. Microw. Conf.*, Paris, France, 24-26 Sept. 2024.

[18] J. Hou, G. Goussetis, J. S. Thompson and Y. Ding, "Eigenvector Informed Precoder Design for Active MIMO Transmitters," *Proc. 55th Eur. Microw. Conf.*, Utrecht, The Netherlands, 23-25 Sept. 2025.

[19] J. Hou, Y. Ding, G. Goussetis and S. Podilchak, "Waveform Synthesis for Active Loadpulling Mitigation in Multiuser MIMO Transmitters," *Proc. 55th Eur. Microw. Conf.*, Utrecht, The Netherlands, 23-25 Sept. 2025.

[20] CVX Research, Inc., *CVX: Matlab Software for Disciplined Convex Programming*, Version 2.0, Aug. 2012 [Online:https://cvxr.com/cvx].

[21] H. Steyskal and J. S. Herd, "Mutual coupling compensation in small array antennas," *IEEE Trans. on Antennas Propag.*, vol. 38, no. 12, Dec. 1990, pp. 1971-1975.

[22] F. Belfiori, S. Monni, W. Van Rossum and P. Hoogeboom, "Mutual coupling compensation applied to a uniform circular array," *11-th Int. Radar Symp.*, Vilnius, Lithuania, 16-18 June 2010.

[23] C. Pfeiffer, F. Dagefu, B. Tomasic, J. N. Twigg and B. -I. Wu, "Virtual Impedance Method for Mutual Coupling Compensation," *IEEE Trans.*

Antennas Propag., vol. 69, no. 8, Aug. 2021, pp. 4569-4579, doi: 10.1109/TAP.2021.3060129.
[24] N. Llombart, A. Neto, G. Gerini and P. de Maagt, "Planar circularly symmetric EBG structures for reducing surface waves in printed antennas," *IEEE Trans. Antennas Propag.*, vol. 53, no. 10, Oct. 2005, pp. 3210-3218.
[25] P. Hannan, "The element-gain paradox for a phased-array antenna," *IEEE Trans. Antennas Propag.*, vol. 12, no. 4, July 1964, pp. .423-433, doi: 10.1109/TAP.1964.1138237.
[26] J. E. Roy and L. Shafai, "Generalization of the Ludwig-3 Definition for Linear Co-polarization and Cross Polarization," in *Proc. 1996 Symp. Antenna Tech. Applied Electromag.*, 6-9 August 1996, Montreal, Canada.
[27] R. Casero, *Matlab implementation of local minima search named findpeaksn.m*, Univ. Oxford, UK, 2012. [Online: https://searchcode.com/file/343055682/matlab/PointsToolbox/findpeaksn.m/]
[28] H. Lyu and K. Chen, "Balanced-to-doherty mode-reconfigurable power amplifier with high efficiency and linearity against load mismatch," *IEEE Trans. Microw. Theory Tech.*, vol. 68, no. 5, May 2020, pp. 1717-1728, doi: 10.1109/TMTT.2020.2979844.
[29] H. Lyu, Y. Cao and K. Chen, "Linearity-enhanced quasi-balanced Doherty power amplifier with mismatch resilience through series/parallel reconfiguration for massive MIMO," *IEEE Transactions on Microwave Theory and Techniques*, vol. 69, no. 4, April 2021, pp. 2319-2335, doi: 10.1109/TMTT.2021.3056488.
[30] W. H. Doherty, "A new high efficiency power amplifier for modulated waves," *Proc. Inst. Radio Engineers*, vol. 24, no. 9, Sept. 1936, pp. 1163-1182, doi: 10.1109/JRPROC.1936.228468.
[31] S. Hu, S. Kousai and H. Wang, "Antenna impedance variation compensation by exploiting a digital Doherty power amplifier architecture," *IEEE Trans. Microw. Theory Tech*, vol. 63, no. 2, Feb. 2015, pp. 580-597, doi: 10.1109/TMTT.2014.2385860.

Chrysovalantis Stefopoulos received his M.Sc. degree in Electrical and Computer Engineering from Aristotle University of Thessaloniki, Greece, in 2022. Following his studies, he undertook a nine-month internship in the Radar Technology department of the Netherlands Organisation for Applied Scientific Research (TNO), The Hague, The Netherlands. After completing his internship, he joined the Antenna group within the same department, where he currently works as an Electromagnetic (EM) and Antenna Engineer. His research interests include antenna design for space applications, optimization techniques for antenna beam forming, and filter design, with a particular focus on 3D integrated passive device (IPD) technology for packaging applications.

Peter de Hek (M'07) was born in Hardinxveld-Giessendam, The Netherlands, in 1963. He received the B.Sc. degree in electrical engineering from Dordrecht Polytechnic, Dordrecht, The Netherlands, in 1985. His bachelor's thesis dealt with communication between a number of mainframe computers. After fulfilling his service in the Dutch Army, he joined the TNO Physics and Electronics Laboratory, The Hague, The Netherlands, in 1987, where he started working on the characterization and design of antennas. Since 1990, he has been involved in the design and characterization of monolithic microwave integrated circuits. He has been a Project Leader in a number of international projects. These projects involve the design of power amplifiers in MESFET, HFET, and HBT technologies. Mr. de Hek was the recipient of the Prize for the Best Oral Paper presented during the GAAS/EuMW Conference in 2001.

Mario Coutino received the M.Sc. and Ph.D. degree (cum laude) in electrical engineering from the Delft University of Technology, Delft, The Netherlands, in July 2016 and April 2021, respectively. Since 2020, he has been a Signal Processing and Machine Learning Researcher with the Radar Technology Department of the Netherlands Organisation for Applied Scientific Research (TNO). He has held temporally positions with Thales Netherlands, during 2015, and Bang & Olufsen, during 2016. His research interests include array signal processing, signal processing on networks, optimization, numerical linear algebra, machine learning and radar

Dave Bekers (Senior Member, IEEE) received the M.Sc. degree in mathematics and the P.D.Eng. and Ph.D. degrees from the Technische Universiteit Eindhoven, Eindhoven, The Netherlands, in 1999, 2001, and 2004, respectively. He carried out his final project for the post-graduate program "Mathematics for Industry" and his Ph.D. project with Thales Nederland, Hengelo, The Netherlands, in the field of array antennas.,Since November 2004, he has been with TNO, The Hague, The Netherlands, organization for applied scientific research, where he first worked in antenna design, modeling, and simulation, and guided a few projects in the field of mm-wave and THz antenna technology. In the past ten to thirteen years, he worked mainly in the fields of radar signal processing and phased-array antennas on topics such as beamforming, target detection, parameter estimation, and novel waveforms. Additionally, he had the technical guidance at TNO for a few activities carried out within D-RACE, the Dutch Radar Centre of Expertise, a strategic alliance between TNO and Thales Nederland B.V.

Ioannis Iliopoulos received the Diploma of ectrical and computer engineering from the Aristotle University of Thessaloniki, Thessaloniki, Greece, in 2013, and the Ph.D. degree from the Institut d'Electronique et de Télécommunications de Rennes (IETR), Université de Rennes 1, Rennes, France, in 2017. He conducted his master's thesis at the Laboratory of Electromagnetics and Acoustics (LEMA), École Polytechnique Fédérale de Lausanne (EPFL), Lausanne, Switzerland, where he researched on antenna near-field topics until 2014. He was a Post-Doctoral Fellow with Université de Rennes 1, where he conducting research on bioelectromagnetics until 2018. In the framework of his PhD thesis, he spent 6 months at the Microwave Lab, University of Pavia, Pavia, Italy, supported by the Italian Association for Cancer Research (AIRC). He is currently researcher at the Netherlands Organization for Applied Scientific Research (TNO), The Hague, The Netherlands. His current research interests include analysis and design aspects of phased arrays for radar applications.

Stefania Monni (S'01–M'06) received the M.Sc. degree (cum laude) in electronic engineering from the University of Cagliari, Cagliari, Italy, in 1999, and the Ph.D. degree in electronic engineering from the Technical University of Eindhoven, The Netherlands, in 2005. From 1999 to 2000, she was a trainee with the Radio Frequency System Division, European Space Research and Technology Centre (ESA-ESTEC). Currently, she is a senior scientist at TNO Radar Technology department. Since 2014 she leads the Antenna team, where she is responsible for the definition and technical coordination of the research activities and for the long term strategy. Since 2018 she is also a senior scientist at the Chip Integration Technology Centre, RF Packaging Program. In 2024 she joined the Technical University of Eindhoven as part-time professor on array antenna technologies for radar systems. Since 2022 Stefania is the President of the European Association on Antennas and Propagation. Her research interests include active array antennas, Frequency Selective Surfaces and advanced manufacturing technologies.